

# Light Responsive Protective Coatings†

Ekaterina V. Skorb,<sup>\*a</sup> Dmitry V. Sviridov,<sup>b</sup> Helmuth Möhwald<sup>a</sup> and Dmitry G. Shchukin<sup>a</sup>

## Supporting Information

*Preparation of photosensitive nanocontainers.* Mesoporous titania was synthesized by oxidation of titanium carbide in 5 M nitric oxide according to the procedure similar to that proposed in Ref. S1 with the following ultrasound treatment. Thus obtained titania dispersion has a BET surface of 529 m<sup>2</sup>/g and exhibits a N<sub>2</sub> adsorption – desorption isotherm of IV type with H3-type hysteresis loop according to the Brunauer classification. The type of isotherm points to the formation of an interconnected mesoporous system with high pore connectivity level. The pore size distribution obtained from the isotherm evidences that pores are distributed within a narrow range between 2 and 12 nm with average pore diameter of ca. 5 nm. The XRD analysis shows that the titania network is built of crystallites with average size of ca. 3 nm.

The loading of the mesoporous particles with corrosion inhibitor was carried out by evacuation of the titania suspension in benzotriazole solution (50 mg/ml). The loading was performed several times to attain saturation. During the first two loading cycles the weight of the porous cores gradually increased with a loading increment of ~ 30-35 mg of benzotriazole per 1 g of titania. The saturation corresponding to complete filling of the inner porous space was achieved after the fifth loading step. The TEM images of titania particles used as the cores for containers are presented in Fig. S1.

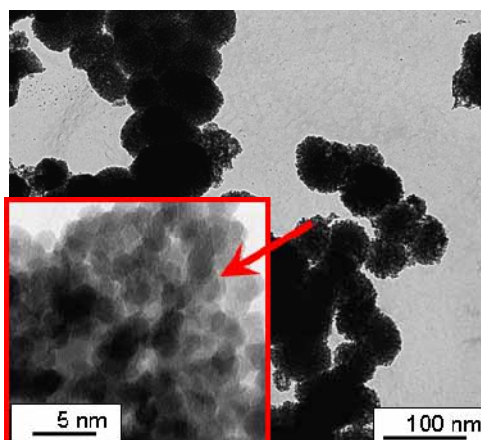


**Fig. S1** TEM images of porous titania particles.

The polyelectrolyte shells were deposited over the cores via the LbL deposition route. Since the particles of meso-TiO<sub>2</sub> are negatively charged, a layer of polyethyleneimine (PEI, MW~600000-1000000) was applied first from PEI solution. Then, after thorough washing with the use of centrifugation the deposition of negatively-charged poly(sodium 4-styrenesulfonate) (PSS, MW~70000) was performed. These deposition procedures were repeated two times yielding containers with the shell consisting of two PEI/PSS bilayers which were used for corrosion healing experiments. For optical experiments the shell involving three bilayers was used that facilitates container aggregation; as the result, micron-sized container aggregates well recognized by optical microscopic technique were obtained.

Mesoporous silica cores (average size of 200 nm, average pore size of 3 nm) used for comparison as the non-photosensitive containers were synthesized via Ref. [S2]. Loading with benzotriazole and deposition of polyelectrolyte shell were performed according the protocol similar to that described above.

**Preparation of light-controllable coatings** The hybrid zirconia-organosilica films used as the carriers of TiO<sub>2</sub>-based nanocontainers were prepared using the controllable sol-gel route [S3] by mixing in 1:2 volume ratio the following sols: (i) zirconia sol obtained by hydrolyzing 70 wt% zirconium *n*-propoxide in propan-1-ol mixed with ethylacetacetate (1:1 volume ratio) and (ii) organosiloxane sol synthesized by hydrolyzing 3-glycidoxypropyltrimethoxysilane in propan-2-ol (in both cases acidified water at pH 1 was used to initiate the hydrolysis). The final sol-gel mixture was stirred under ultrasonic agitation for 60 min and then aged for 1 hour at room temperature. The loaded nanocontainers were added to zirconia sol before mixing with organosiloxane sol and the resultant mixture was then used for dip-coating. The rate of substrate withdrawal was 18 cm/min. The coated samples were allowed to hang vertically in ambient conditions for 45 min and then cured at 130°C for 1 hour. The thickness of the film was ~1.5 μm as evidenced using edge on AFM.

**SVET measurements** SVET measurements were performed using equipment purchased from Applicable Electronics (USA). Diameter of the Pt blackened electrode tip was 20 μm, the peak-to-peak amplitude was 60 μm, and the vibration frequency was 655 Hz. An area of 4.5×4.5 mm<sup>2</sup> was scanned with a step width of 150 μm. The probe was 300 μm above the sample surface. The scans had duration of ca. 15 min each and were repeated every ½ hour. All the potentials were measured against Ag/AgCl, Cl<sup>-</sup>(sat.) reference electrode (0.201 V versus NHE). To initiate corrosion process, the mechanical defect was created at the surface of the coating before immersion of the sample into the corroding solution (0.1 M NaCl). The 3D current maps obtained by SVET permit to trace the development of corrosion process at the surface of bare AA2024 and AA2024 plates with SiO<sub>x</sub>:ZrO<sub>x</sub> coating during the treatment of the sample in sodium chloride solution (Fig. S2).

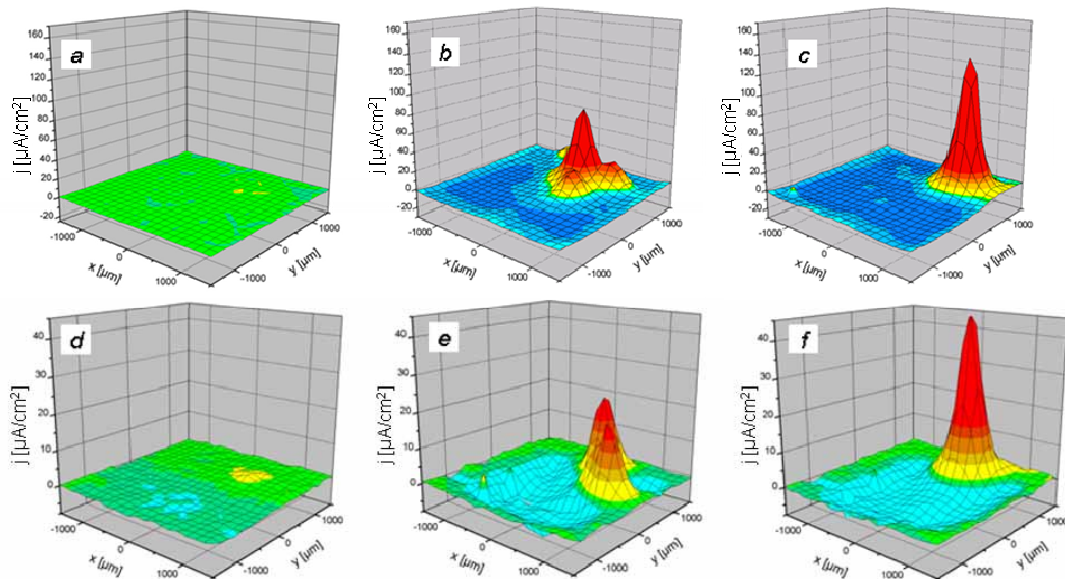


**Fig. S2** a-f) Scanning vibrating electrode measurements (SVET) of the ionic currents above the surface of (a-c) AA2024 and (d-f) AA2024 covered with sol-gel film. (a,d) beginning moment; (b,e) 42 hours of immersion; (c,f) 60 hours of immersion. Solution: 0.1 M NaCl. Note the different scales!

*Photostability of  $\text{SiO}_x\text{:ZrO}_x$  sol-gel films.* Fig. S3 shows the metamorphoses of IR spectra of sol-gel film loaded with meso- $\text{TiO}_2$  (titania cores without polyelectrolyte shells) during the long-term UV light irradiation. The band at  $1720 \text{ cm}^{-1}$  exhibiting gradual development during the first hour of illumination corresponds to the oxidation of the glycerol groups at the surface of the zirconia- organosiloxane matrix. Further illumination does not result in any changes in the IR spectra. The photocatalytic reactions occurring at the surface of sol-gel film do not affect the matrix bonds, which confirms the necessary matrix stability under irradiation.

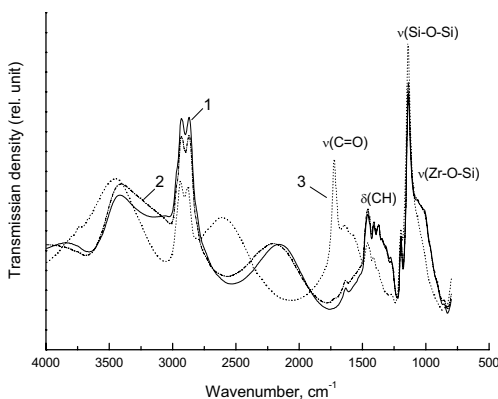


**Fig. S3** IRRAS spectra for film  $\text{TiO}_2\text{-SiO}_x\text{:ZrO}_x$  during UV-irradiation in air condition: 1 – initial spectrum; 2 – after 30 min of irradiation; 3 – after 4 hours of irradiation.

*AFM images of the nanocontainer-coatings* The AFM image given in Fig. S4 points to the uniform distribution of the embedded containers for comparison the AFM image of bare  $\text{SiO}_x\text{:ZrO}_x$  hybrid film.

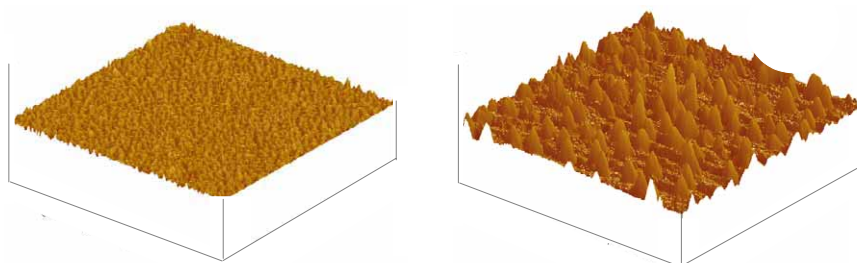


**Fig. S4** Atomic Force Microscopic (AFM) images of (a)  $\text{SiO}_x\text{:ZrO}_x$  hybrid film of (b)  $\text{SiO}_x\text{:ZrO}_x$  hybrid film with the embedded containers  $\text{TiO}_2/\text{PEI}/\text{PSS}/\text{PEI}/\text{PSS}$  of polyelectrolyte titania based nanocontainers incorporated into a  $\text{SiO}_x\text{:ZrO}_x$  hybrid film. Areas  $1.5 \times 1.5 \mu\text{m}$ .

*Container opening experiments.* For UV light illumination of the samples both 365-nm of 120 W high-pressure Hg lamp (intensity  $15 \text{ mW/cm}^2$ ) or the  $\text{Nd}^{3+}\text{:YAG}$  laser (the third harmonic, 354 nm) were used. In the latter case the laser beam was scanned over the surface of the sample and the release of the probing dye stored in the containers was traced by confocal microscopy (Leica TCS SP inverted confocal microscope system, Germany). The local opening of containers by near IR and visible light was performed by employing a homemade laser setup in which a collimated pulsed laser (time duration 0.7 ns, and power  $0.1 \mu\text{J}$ , 820 nm or 532 nm) was focused onto the sample through a microscope objective ( $\times 100$ ) and the transmission images were recorded by a charge-coupled device camera connected to a computer. The laser intensity was measured by a Newport-1830C power meter.

*Blank experiments* No healing effects were observed (i) upon IR illumination of sol-gel coatings loaded with titania containers (Figure S5ab); upon UV illumination of sol-gel coatings loaded with silica-based containers (Figure S5cd)

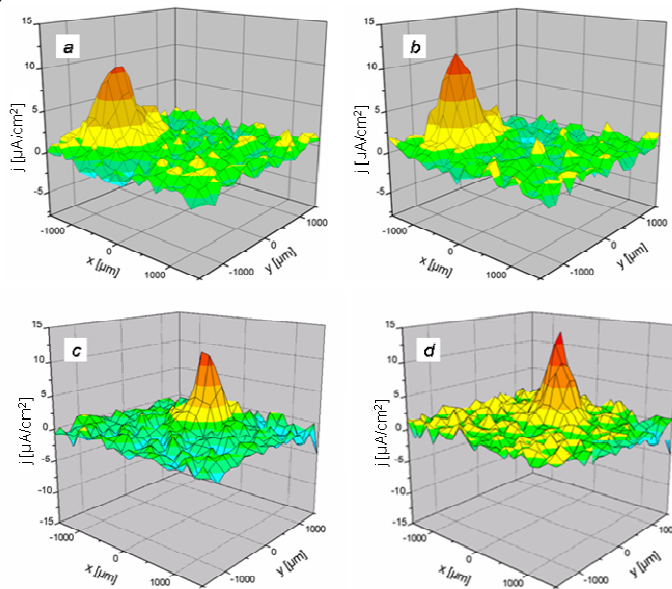


**Fig. S5** SVET of the ionic currents above the surface with  $\text{TiO}_2$ (benzotriazole)/(PEI/PSS)<sub>2</sub> containers (a) after 64 hours of corrosion; (b) after IR-irradiation; and  $\text{SiO}_2$ (benzotriazole)/(PEI/PSS)<sub>2</sub> containers (c) after 64 hours of corrosion; (d) after UV-irradiation. Solution: 0.1 M NaCl.

*The absence of containers "leaking".* Diagram shown in Fig. S6 has been done based on the absorption spectra in the ultraviolet and visible range which were recorded to determine benzotriazole concentration during release by means of an Agilent 8453 spectrophotometer (Agilent Technologies, USA). It is seen that the release of benzotriazole was achieved just in the two: in the case of UV irradiation of titania based containers and in the case of IR irradiation of  $\text{TiO}_2/\text{Ag}$  based containers. Spontaneous release was not found for non-irradiated coatings

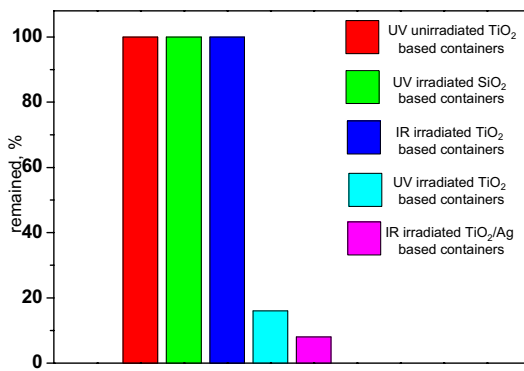


**Fig. S6** Diagram of the quantity of remained benzotriazole inside the containers: as UV souse the 365 nm-line of a 120 W high-pressure Hg lamp was used, time of irradiation was 5 min; as IR souse homemade laser setup was used release occurs after exposure to a single pulse.

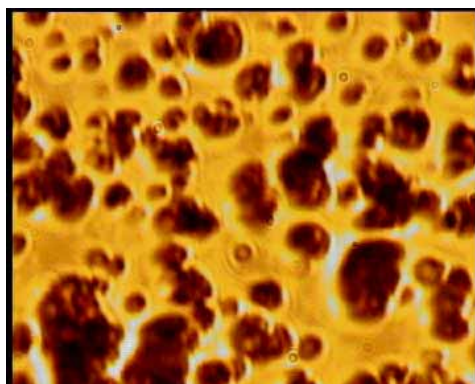
*Video of IR light stimuli opening of Ag-modified nanocontainers.* Video S1 demonstrates the container opening induced by a single pulse of near IR laser.



**Video S1.** Video corresponds to the on-line irradiation of  $\text{TiO}_2:\text{Ag}$  (Rhodamine 6G)/(PEI/PSS)<sub>3</sub> containers in  $\text{SiO}_x:\text{ZrO}_x$  film using a homemade laser setup in which a collimated pulsed laser (time duration 700 ps, and power 3  $\mu\text{J}$ , 820 nm) was focused onto the sample. The particles observed in the video correspond to the container aggregates.

*Video of visible light stimuli opening of Ag-modified nanocontainers*

Video S2 demonstrates the container opening induced by a single pulse of visible laser.



**Video S2.** Video corresponds to the on-line irradiation of  $\text{TiO}_2:\text{Ag}$  (Rhodamine 6G)/(PEI/PSS)<sub>3</sub> containers in  $\text{SiO}_x:\text{ZrO}_x$  film using a homemade laser setup in which a collimated pulsed laser (time duration 700 ps, and power 3  $\mu\text{J}$ , 532 nm) was focused onto the sample. The particles observed in the video correspond to the container aggregates.

## References

- [S1] D.-L. Shieh, J.-S. Li., *Micropor. Mesopor. Mater.* **2007**, *98*, 339-343;
- [S2] N. Thanabodeekij, S. Sadthayanon, E. Gulari, S. Wongkasemjit, *Mater. Chem. Phys.* **2006**, *98*, 131-137;
- [S3] D.G. Shchukin, M. Zheludkevich, H. Möhwald, *J. Mater. Chem.* **2006**, *16*, 4561-4566.